Bergen Center for Computational Science

BCCS
TECHNICAL REPORT SERIES

Natural seabed seeps, preparations for numerical studies

Lars Inge Enstad

REPORT No. -22 **March 2007**

UNIFOB
the University of Bergen research company

BERGEN, NORWAY

BCCS Technical Report Series is available at http://www.bccs.no/publications/

Requests for paper copies of this report can be sent to:

Bergen Center for Computational Science, Høyteknologisenteret,
Thormøhlensgate 55, N-5008 Bergen, Norway

Natural seabed seeps, preparations for numerical studies

Lars Inge Enstad *

Computational Math Unit
Bergen Center for Computational Science
Geophysical Institute Jahnebakken 3
N-5008 Bergen
Norway

October 10, 2007

*Email: lars.inge.enstad@bccs.uib.no, WWW: http://www.bccs.no/

Contents

1 Introduction **3**

2 Known locations of CO_2 leakage **3**
2.1 Jade field, Okinawa through, . . . 3
2.2 Champagne field, Mariana Arc, . . . 4
2.3 Yonaguni Knoll IV, Okinawa Trough . . . 4
2.4 Loihi Seamount, Hawaii . . . 5
2.5 Hellenic Volcanic Arc . . . 5
2.6 Kagoshima Bay . . . 5
2.7 Chirikov Basin and Norton Sound, Offshore Alaska . . . 5
2.8 Panarea area, Sicilia . . . 6

3 Hydrocarbon leakage from pockmarks **6**
3.1 Short on history . . . 6
3.2 Features of pockmarks . . . 6
3.3 Geological conditions . . . 7
3.4 Time development of pockmarks . . . 7
3.5 Anthropogenic CH_4 seep near 58^o N, 1^o40' E in the North Sea . . . 8

4 Discussion **8**
4.1 Flux through hydrate layer . . . 8
4.1.1 Hydrate in suspension . . . 8
4.1.2 Micro perforated plate models . . . 8
4.1.3 Permeable solid plate models . . . 9
4.1.4 Aspects of the Hydrate-Sediment layer . . . 9
4.2 Properties of CH_4 in seawater . . . 9
4.2.1 Density of pure CO_2 and CH_4 . . . 9
4.2.2 Solubilities . . . 10
4.2.3 Density of seawater containing dissolved spices . . . 11
4.2.4 Dissolution rate . . . 11
4.2.5 Hydrate Stability Zone . . . 13
4.2.6 Diffusivity and viscosity . . . 13
4.2.7 Bacteria oxidation of CH_4 . . . 13
4.3 Observations of Methane plumes . . . 14
4.3.1 Methane and Carbon Dioxide bubbles . . . 15
4.4 Droplet modelling . . . 17
4.5 Summary and preliminary conclusions . . . 17
4.6 Advantages and disadvantages . . . 18

1 Introduction

Leakage at the seafloor of liquids and gases has been observed and studied during the last four decades. Such environments provide conditions for unique ecosystems in it's surroundings, and affects the chemical and physical state of the ocean. In a new project funded by VISTA we aim to design and implement a numerical model for seepage through the seafloor by simulating the gas flow both in the ground, in the seawaters and the interface between them. Such seepages can act as natural laboratories for studying the release, dissolution and transport of gases in seawaters. By combining computational efforts with observation one can obtain a better understanding for these processes.

Two types of seepages are considered in this report. The known locations and features of CO_2 leakages near hydrothermal vents are listed and discussed together with a discussion on pockmarks found in the North Sea. There is also a discussion on the advantages and disadvantages by the two types of seeps in the context of relevance to leakage and spreading of CO_2 from geological reservoirs. In this regard the properties of CO_2 and CH_4 in seawaters is compared, and previously observations of behaviour of CO_2 and CH_4 droplets/bubbles is discussed. In addition a single droplet/bubble model is employed to give a more quantitative impression of the differences. Some reports on observations of spreading of CH_4 plumes is presented to give some preliminary conclusions based on the discussion.

2 Known locations of CO_2 leakage

To our knowledge the literature reports on four locations with liquid CO_2 leakage. In addition there are several locations of shallower CO_2 seepages. These are all located in volcanic areas with hydrothermal venting where other gases and minerals also is vented to the seawaters. In the following we give a short description on the different findings with emphasis on matters relevant for modelling.

The reports of gas CO_2 leakage from some places around the world in this section is gathered from Judd and Hovland [2007].

2.1 Jade field, Okinawa through,

Sakai et al. [1990]

This CO_2 leakage was discovered in 1989, and is located within the Jade field at a depth of 1300 to 1550 meters depth. This is a hydrothermal field 1000 meters by 200 meters, and consists of active and inactive chimneys and mounds. The hydrothermal fluid is found to have a temperature between 220 ^{o}C and 320 ^{o}C. Two locations was confirmed to form CO_2 bubbles. These were 2 to 5 meters in diameter and were shaped as subcircular regions with yellowish white alteration zones. The fluid bubbling up from the sediments was found to consist of 86 % CO_2 , 3 % H_2S and 11 % residual gas (CH_4 + H_2). When the CO_2 rich fluid seeped through the sediments it often formed a translucent elongated conical pipe which was approximately 10 cm long and 1 cm in top diameter. Sakai *et al.* Observed these cones to be standing on the sea floor while the CO_2 rich fluid bubbled through the top of the cone. After a while the bubbling ceased and after around a second either the bubbling resumed or the whole cone was carried away.

The chemical composition of C, S and He isotopic ratios indicate that the CO_2 rich fluid has the same origin as a nearby black smoker. Since the concentration of CO_2 in the hydrothermal solution is much smaller than the saturation concentration in water at these depths and temperatures, the authors speculate on two different explanations on how the CO_2 rich liquid is separated. The first uses the fact that the upward CO_2 flux will fluctuate during a volcanic cycle and the concentration of CO_2 will increase significantly in the hydrothermal solution. Also the temperature is close to the boiling point of the solution.

These two factors together can create vapour phase with a sufficiently high concentration of CO_2 which can create the CO_2 rich fluid upon cooling. The second assumes that CO_2 rich fluid can be contained in vesicles, and when these are released in pore water and when appropriate conditions prevail, pore water could be saturated with CO_2. This effect could lead to separation of CO_2.

The two phase CO_2 rich and H_2O rich fluids will go upward driven by buoyancy. When the temperature becomes lower than 10 ^oC hydrate will form. This hydrate will prevent the flow of CO_2 rich fluid, and hence lead to an accumulation of CO_2 at shallow depth. The paper by Sakai does not include an estimation of the amount of CO_2 leaked at the Jade field.

2.2 Champagne field, Mariana Arc,

Lupton et al. [2006]

The Champagne field was discovered in 2004. The field lies at a depth of 1600 meters nearby a volcano called NW Eifuku and consists of small white chimneys. This is a place of converging tectonic plates. The CO_2 leakage is located approximately 80 meters WNW of the volcano summit and the leakage point is around 10 m^2. The area of bubbling of CO_2 rich fluid consists of pumice and whitish/yellowish sulphur-rich material. From the chimneys buoyant milky white fluid flows into the seawaters. Around the chimneys droplets coated with hydrate emerge from the bottom. The CO_2 rich fluid consists of 98 % CO_2, 1 % H_2S and only trace amounts of CH_4 and H_2. The hydrothermal fluid venting from the white chimneys is 103 ^oC, and the droplets is < 4 ^oC. It was not observed hydrate cones as found at the Jade field by Sakai *et al.*

The vent fluid contains around 3.0 moles/kg of CO_2 which is an order of magnitude larger than any previously CO_2 values reported. In fact the solubility of CO_2 at these pressure and temperature conditions is around 1 mole/kg. The conclusions of the authors based on extrapolation of the temperature and fluid composition to a zero-magnesium value, are that the Champagne field is not a high temperature H_2O system, but rather a high temperature CO_2 system. The authors also suggest that there exists a layer of CO_2 capped by a hydrate layer beneath the sea bottom. It is speculated that the vent fluid is entraining small amounts of CO_2 from this layer and this leads to the high CO_2 levels. The CO_2 gas will cool as it ascends from its magmatic origin and may entrain small amounts of water. Water and CO_2 is thought to be immiscible at these pressure and temperature conditions, and hence the water and CO_2 will flow separately.

The amount of CO_2 arising from the Champagne field was estimated by the authors by counting droplets rising from the bottom. They found around 300 droplet streams each releasing 2 droplets s^{-1} and each with a diameter of 1.5 cm. This gives a total liquid CO_2 flux of 1 litres s^{-1} or 1 kg s^{-1}.

2.3 Yonaguni Knoll IV, Okinawa Trough

Inagaki et al. [2006],Konno et al. [2006]

This site was found in 2003. The main focus of Konno et al. is to reveal the subseafloor processes. Therefore the article describes the chemical features of the fluids leaked at the site. The highest temperature observed is 325 ^oC. As the two other papers they find that the CO_2 rich fluid must originate from the vent fluid because of the similar chemical properties. They conclude that the CO_2 is separated from the vent fluid by boiling. When the vapour phase cools hydrate is created and this hydrate is assumed to melt to form liquid CO_2 due to a temperature increase within the sedimentary layer.

Inagaki et al. performed investigations in the same area as Konno et al. Under expeditions to the Yonaguni Knoll hydrothermal field they discovered a CO_2 lake 50 meters southward from the hydrothermal vents, down a gentle slope at 1380 meters depth. The

lake was larger than 200 m^2 , and small droplets of CO_2 were leaking from the lake. Samples were taken from the leaking fluid and the chemical composition was found to be 85.1 % CO_2 and 13.95 % CH_4. The hydrogen concentrations were below the detection limit. At the seafloor the temperature was found to be 3.9 ^oC, and 35 cm into the sediments it was found to be 9.9 ^oC. Core samples were taken from the area of the lake and analysed. It was found that the sediment cover was around 20-40 cm thick. Below a layer of CO_2 hydrate was found which was around 10 cm thick. Also pH was measured and found to be 6.6 in the porewater of the core and 6.3 in the pavement samples. An interesting feature of the samples was the finding of microbes. The authors speculate whether the microbial processes can contribute to the sediment consolidation and capping of the CO_2 lake.

2.4 Loihi Seamount, Hawaii

35 km south of the island Hawaii a hydrothermal vent system at Loihi Seamount emit 5000-100 000 t yr^{-1} of CO_2. This site is used as a natural laboratory for the impact of released CO_2 to seawaters on the ecosystem in the vicinity of the release point Vetter and Smith [2005]. The site is located at water depths of 1200 - 1300 meters. The temperature of the vent fluids is measured to < 31 ^oC. The large amount of CO_2 emitted gives local pH levels as low as from 4.2 - 4.4 (Karl et al. [1988], Sedwick et al. [1992]) and CO_2 concentration of as high 418 mol m^{-3}. The relatively low temperature of the venting fluid and high CO_2 concentrations gives the effect that the plume approaches background levels over spatial scales of meters whereas the CO_2 concentrations remain high.

2.5 Hellenic Volcanic Arc

In the vicinity of some of the Greek Islands (e.g. Kos, Lesbos, Methana, Milos Nisiros etc.) there is a system of hydrothermal venting. In these areas large volumes of gas is emitted, and a large fraction of this gas is found to be CO_2. The temperature at these hydrothermal vents is generally below 150 ^oC. At one of the locations (i.e. Milos) the gas flow rates were measured from 0.1 to 56.6 l h^{-1} whereas at the location Kos the gas flow rate ranged from 1.7 to 65.2 l h^{-1}. These leakage points are rather shallow with one of the deepest found at 110 m depth south of Milos. By surveying an area of 34 km^2 Dando et al. [1995] found that gas venting occurs at several places in this area. The total flux from these locations has been estimated to 2×10^{11} l y^{-1}. These leakage points is part of a hydrothermal venting system where water is entrained into the seabottom in a "recharging" zone and is dissolving different gases and minerals before rising to the seafloor again due to convection and is released through the sea bottom again.

2.6 Kagoshima Bay

This is an area not so extensively described in the literature following Judd and Hovland [2007]. The bay harbour an active volcano called Mount Sakurajima which separates two volcanic calderas. Here cold seeps and shallow (at 80 to 200 m depth) hydrothermal venting are found. The gas consists mostly of CO_2 (80.6% to 84.3%) with a fraction of 12.5% to 15.3% of CH_4 and traces of H_2S. The pH is measured to 5.1 to 6.9, and the temperature is found to be 28 to 30 ^oC.

2.7 Chirikov Basin and Norton Sound, Offshore Alaska

An interesting seep site offshore Alaska has been studied by Nelson et al. [1979], Kvenvolden et al. [1979]. This location is on the shallow shelf adjacent to Alaska with water depths between 20 m to 50 m. In this area "turbidity on boomer records and the total disruption of reflections on sparker records suggest that there is gas containing sediments over an area of 50 km^2". Also observations on echo sounder suggest the presence of seeps. On

the seafloor it is not found pockmarks, but deep conical pits 10-40 cm in diameter. The pits have been observed along a 1 km video transverse. These pits are described to "contain vertical holes descending to unknown depths". Following Judd and Hovland [2007] they can not be found on side scan sonar because they are too small. By analysing the gas from these pits it was found that they contain 98% CO_2 and only a small fraction of CH_4.

2.8 Panarea area, Sicilia

In the Panarea area outside Sicilia there is a hydrothermal vent area with leakage of CO_2 gas. In this volcanic area gas is seeping up from 20 meters depth at different rates. This area has been studied with the aim to clarify the effects of CO_2 bubbling on pH levels and biota. Hence this area is used as a natural laboratory for CO_2 leaking in to the seawaters. There is also plans from NIVA to develop a modelling tool for the area.

3 Hydrocarbon leakage from pockmarks

This chapter is written based on Hovland and Judd [1988]

3.1 Short on history

Pockmarks are small depressions or "craters" on the seafloor. Observations indicates that they are found in areas where fluid or gas is seeping up through the seabed. Pockmarks are dependent on soft sediments to form. This seepage can be anything between vigorous bubbling of gas from the seabed to only slow seepage of micro bubbles or hydrocarbon compounds in solution.

The first seabed pockmark was discovered in 1970 by King and MacLean [1970] at the continental shelf of Nova Scotia outside Canada. This was made possible by the introduction of the side-scan sonar. The same year pockmarks were discovered in the North Sea, and since 1978 Statoil has run the most extensive and continuous project to elaborate pockmarks. Because of this the North Sea is a better mapped area by side-scan sonar than any other continental shelves in the world. Because pockmarks are manifestations of gas leakage in the sediments they are dependent on soft sediments on the sea bottom to occur. In the North Sea such sediments are mainly present in the Norwegian Trench and the North Sea Plateau.

3.2 Features of pockmarks

Since the type of sediments and their permeability is varying the numbers of pockmarks per square kilometre can go from 0 to 60 when counting only those which are more than 10 meters across. The general size of pockmarks are 50 to 100 meters in diameter and they have depths between 2-3 meters, but the size can also vary greatly. The shapes of the pockmarks can go from circular to more elongated pockmarks.

Some of the features of the gas leakage within the pockmark have been revealed by studies with ROVs (Remotely Operated Vehicle). Usually each leakage occurs as a single stream of bubbles with bubbles of the diameter of 1 cm. These arise from small holes which have the same size as the bubbles and these holes are generally located within a shallow funnel shaped depression approximately 20 cm in diameter. The chemical composition from the gas seepages in pockmarks has also been estimated. 98-99 percent of the gas is found to be methane, but higher hydrocarbons is also found to be present. To our knowledge there are only two studies Leifer et al. [2007], Clark et al. [2000]) (both in the same area outside California) which report on CO_2 from a hydrocarbon leakage. Leifer et al. found the chemical composition to be 84 % CH_4 14 % CO_2 and the rest was mainly higher hydrocarbons whereas Clark et al. found 1.3 % CO_2.

The rate of gas seepage has also been tried estimated on the global scale by e.g. Hovland et al. [1993]. For the global scale the flux per square meter per year is estimated for an area of pockmarks and then integrated up. This is found to be of the order of 13 g m^{-2} yr^{-1} for shallow hydrocarbon-rich areas. By a ROV survey in the Tommeliten Field it was found that a seepage released one bubble every 6 second and that the total production from the main seepage area was around 24 m^3 day^{-1}. The depth at this location was 75 meters with a corresponding ambient pressure. An unusually large pockmark (450 m wide, 700 m long and 17 m deep) was found on the Witch Ground Formation. Three gas seepages were found when surveying the pockmark by a ROV. The rate of seepage was found to be 200 l h^{-1} (4,8 m^3 day^{-1})for the three seepages and possibly for the whole pockmark.

3.3 Geological conditions

A relevant question regarding pockmarks is the origin of the leaking gas. A study by Rensbergen et al. [2007] et al. reports from geological conditions in the Connemara Field in the Porcupine Basin outside Ireland. They conclude that there is fluid migration pathways all the way from 1.5 km below the seabottom. By analysing the isotopic values and looking at the ratios of methane/ethane and propane it has been concluded that most of the gas is of thermogenic origin and therefore has migrated from deep source rock. The migration is characterised by focused flow in the deep layer, but as the fluid is closer to the seafloor the flow becomes diffuse. The authors state that there is no direct relationship between the underground escaping route and the seafloor distribution of pockmarks, and the distribution is more or less random.

At appropriate temperature and pressure conditions methane together with water is known to form hydrate or clathrate. Such conditions is found in most of the world's oceans at depths greater than a few hundred meters. A relevant question is therefore if some of the methane leaking out through pockmarks has its origin from hydrate deposits, or is temporarily stored as gas hydrate on its way to the sea bottom. At the Vøring Plateau outside the cost of mid Norway a pockmark field was found by Ivanov et al. [2007]. The pockmarks are large, 100 to 300 meters in diameter, and oval in shape. By taking core samples in this area hydrate was found in the sediments. By using side scan sonar local brightening of some reflectors and attenuation of others showed that there was widespread presence of free gas deeper than 250 meters below the seabed. The authors suggest that gas from below prevent the hydrate from disappearing, and that in periods of low activity flux from the hydrates supports the communities of chemosynthetic biota.

3.4 Time development of pockmarks

In this context it could also be interesting to know something about the creation and time development of the pockmarks. A theory of how pockmarks are formed has been presented in Hovland and Judd [1988]. As fluid from below accumulates in the sediments beneath the sea bed the pore pressure will build up. The overlying rock will not have a uniformly distributed permeability. Also small fractures will form due to the pressure of the underlying gas dome. Eventually the gas will find an escape route through these fractures and result in a violent outburst at the seafloor of gas. Evidence for such process is found e.g. by Zuhlsdorff and Spiess [2004] where they use high-resolution seismic data to show that natural hydraulic fracturing might create permeable pathways for gas. As times goes by gas will seep out, but the pockmark will continue to evolve. In Hovland [2002] it is described how pockmarks develops with time and it speculated that the pockmarks have a self sealing nature. In the upper layer of the sediments O_2 is usually present and oxidation of CH_4 is possible. Further down oxygen-bearing compounds as SO_4^{2-}, NO_3^- and NO_2^- is used as source for microbial activity. Therefore going down from the surface of the seafloor there is a depletion of first O_2 and the the other oxidants. The theory presented in Hovland [2002] assumes microbial activity in the sediments slowly deplete the available O_2 in the upper

layer. When this happens there will be anoxic conditions and H_2S will form. Bacteria is then suspected to colonise parts of the migration conduits in the sediments and this will affect the gas flow. On the top of the pockmark bacterial mats will form and this has been observed at the Tommeliten Field. The seepage will then be a diffusive flow maybe with hydrocarbons dissolved in porewater. This is a self enforcing process because the original conduits is being injected by anoxic and gas-charged porewater. In the last phase carbonate will precipitate and slowly block the escaping routes for the gas and the pockmark will be self sealed.

3.5 Anthropogenic CH_4 seep near 58^o N, $1^o40'$ E in the North Sea

During a cruise in 1994 in the North Sea along 58^o latitude measuring CH_4 concentrations, Rehder et al. [1998] came across high contents of CH_4. These high levels in CH_4 concentrations were a result of a drilling accident in November 1990. By a mistake a shallow gas accumulation was drilled into, and subsequently large amount of CH_4 leaked out. The gas flow rates had decreased strongly after the initial phase, but Rehder et al. [1998] observed a significant seepage still after four years. The authors do not give the precise surface concentration of CH_4 observed near the leakage point, but they did observe concentrations well above 1000 nmol l^{-1} compared to the background levels of 4 nmol l^{-1}. Based on their measurements they were able to estimate the flux of outgassing to the atmosphere from the seepage from 1.20×10^6 to 1.98×10^6 mol d^{-1}. This amounts to 25% of the total outgassing of CH_4 found by the authors for the entire North Sea.

4 Discussion

4.1 Flux through hydrate layer

If one wants to model a CO_2 leakage of the form described in section 2.1 - 2.3 the boundary layer between the CO_2 containing sediments and the ocean would have to be taken into account. As found in all the locations this layer consists of a hydrate layer. A starting point for a model could therefore be the already existing models for flux through hydrate layers. There exists three different physical interpretations on how CO_2 is dissolving through a hydrate layer. In the following we give a short description on these concepts and some strength and weaknesses of the models to give an idea of the state-of-the-art in this research field.

4.1.1 Hydrate in suspension

In this model Shindo et al. [1993] the hydrate layer is thought of as a colloidal suspension of tiny hydrate particles in the liquid CO_2/H_2O phase. The transport through the hydrate layer then becomes a simple case of liquid phase diffusion. This model, however, is in contrast with experimental results which shows that hydrate has a crystalline structure.

4.1.2 Micro perforated plate models

This model Mori and Mochizuki [1997] assumes that there are micro perforations or pores in the hydrate layer. These act as capillaries to transport CO_2/H_2O molecules. This flow is thought to be driven by the pressure induced by the surface tension of the liquid phase that wets the hydrate. Because of the complexity this porous nature of the hydrate layer has not been verified experimentally. Also because of the lack of experimental data there are many unknown quantities such as porosity, diameter of the perforations and tortuosity.

Gas	Molar Mass (gmol^{-1})	Critical Temperature (K)	Critical Pressure (Bar)
CO_2	44.0095	304.2	73.825
CH_4	16.0425	190.6	46.41

Table 1: Different parameters for the two gases treated in this report.

4.1.3 Permeable solid plate models

This concept treats the transport of CO_2 molecules across the hydrate layer as that of diffusion of CO_2 molecules in the crystalline hydrate structure. An important factor in the estimate of the flux based on this model is the diffusivity of CO_2 in the hydrate layer. This parameter was estimated using theoretically study by Demurov et al. [2002] and made it possible for Radhakrishnan et al. [2003] to pursued this model further and compare with experimental results for dissolution from CO_2 droplets.

4.1.4 Aspects of the Hydrate-Sediment layer

The study by Inagaki et al. [2006] shows that under a sediment cover of around 5 cm depth there is a hydrate layer approximately 10 cm deep. It is clear that the sediment in suspension approach will not be suitable for this kind of boundary layer. It is difficult to say with the knowledge at hand if the micro perforated plate model gives a realistic representation of the processes in the sediment/hydrate layer. Apriori it seems to be the most convenient of the models presented above, but the problem arise with the setting of the physical parameters for the model. Also the hydrate layer is much thicker in this case than the hydrate film on which the models have been employed. For the permeable plate model it is assumed that CO_2 can diffuse through the hydrate film without destroying the hydrate cages. It is also assumed that the diffusion is driven by the undersaturated concentration of CO_2 in the seawater. Since the hydrate layer above the CO_2 lake are much thicker than a hydrate film and sediments is present this concept may be difficult to use, and might be erroneously to use for our setting. Also the diffusivity is unknown and may be difficult or impossible to set.

Since the hydrate layer is so different in appearance from the hydrate film that the above mentioned models are used on, the modelling of flux of CO_2 may need another approach, although it may be feasible to use one or more of the known models as a starting point.

4.2 Properties of CH_4 in seawater

The main focus in this part of the discussion will be the behaviour of CO_2 and CH_4 in seawater. We will try to clarify and compare the properties of CH_4 and CO_2 in these environments.

Basically we will compare seven properties of CH_4 and CO_2 in seawater, including the density of the pure gas, solubility in seawater, density of seawater with dissolved gas, dissolution rate of gas into seawater and the hydrate region of the substance, in addition to the viscosity and diffusivity. Other important chemical data are the molecular weight, critical temperature and critical pressure. These are given in Table (1).

4.2.1 Density of pure CO_2 and CH_4

First we look at the density of the pure gases. These are given by equations of state (EOS). In Figure 1 the density of pure CH_4 is given as contour lines in a pressure temperature diagram. To highlight the region from 1 - 40 bar and 273.15 - 283.15 K we have enlarged this region in a new figure. One of the large differences between CH_4 and CO_2 is that CO_2 has a phase transition in seawater at around 500 m depth. CH_4 has no such phase transition in all temperature and pressure ranges found in the ocean. Also CO_2 in liquid

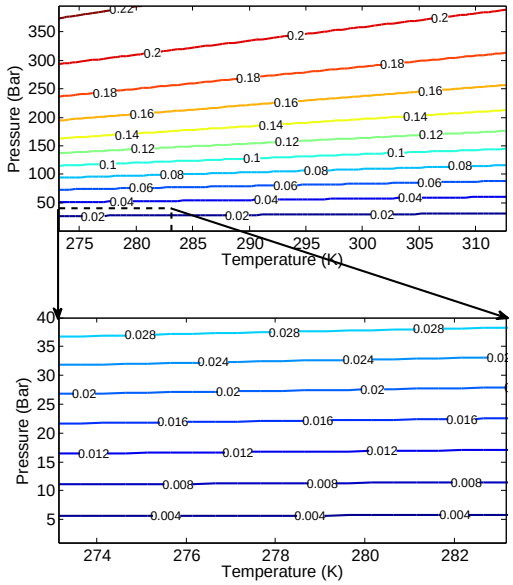

Figure 1: Density $[\mathrm{gcm}^{-3}]$of pure CH_4 as a function of pressure and temperature with a zooming of the region 1 - 40 bar and 273.15 - 283.15 K

phase is more compressible than seawater thus at around 3000 m depth the CO_2 becomes more dense than seawater. To illustrate the difference in the density properties of CO_2 and CH_4 the ratio of the density of the two substances at 4.2 ^{o}C and various pressures is plotted in Figure 2. From this figure it appears that CO_2 is approximately five times heavier than CH_4 in shallow waters with a jump to twenty times heavier when CO_2 becomes a liquid. The ratio decreases to around five again at 4000 meters depth since gases generally is more compressible than liquids.

4.2.2 Solubilities

A recent model by Duan and Mao [2006a] for solubility of CH_4 shows good agreement with experiment so this model is employed to compute data for CH_4. The solubility of CO_2 is estimated following Duan and Mao [2006b]. In Figure 3 the solubility is shown as a function of temperature and pressure. As is usual the solubility increases by pressure and decreases by temperature. There is also added lines to indicate the hydrate region where saturated water will form methane hydrate. In this region the solubilities will be significantly changed. In this region solubilities decrease with pressure but increases with temperature. The difference in hydrate stability region of CO_2 and CH_4 will be discussed in section (5). Also in this section we have enlarged a region for the pressure and temperature ranges for shallow waters. In Figure (4) the ratio of solubility of CO_2 and CH_4 is shown. There is a large difference in the ratio in surface waters compared to deeper waters. The overall conclusion is that solubility of CO_2 is larger and that the ratio ranges from 30 to around 7. This will necessarily lead corresponding higher dissolution rates of CO_2 than

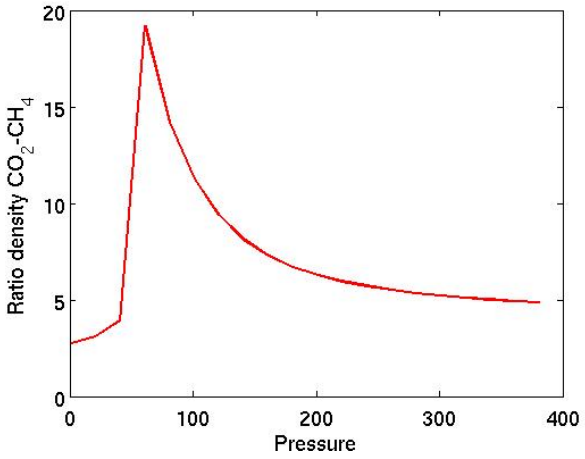

Figure 2: The ratio of the density of pure CO_2 and CH_4 at 277.35 K from 1 - 400 bar.

CH_4 as discussed in the next section.

4.2.3 Density of seawater containing dissolved spices

A simple formula for the extra density introduced by dissolved CO_2 is given as

$$\rho_{sol} = \rho_{seawater} + (M_{CO_2} - \rho_{seawater}\nu_{CO_2})C_T \tag{1}$$

where M_{CO_2} is the molar mass, ν_{CO_2} is the molar volume, C_T is the concentration of CO_2 and $\rho_{seawater}$ is the density of seawater in absence of dissolved CO_2. A similar equation for CH_4 is found in Duan and Mao [2006a]. Unfortunately they do not present the full method for finding the density in seawater, but here we have tried to use the extension for solubility to seawater in an analogues manner. This means that CH_4-monovalent-cation interactions is the same for all cations and that CH_4-bivalent-cation interactions is the double. The anion interactions is neglected. Based on these assumptions we can calculate the effect of dissolved CH_4 and CO_2 on the density of seawaters. The density varies little with pressure and temperature so we use the case when the temperature is 4 ^{o}C and the pressure is 40 bar. The concentration is set to one tenth of an observation by Suess et al. [1999] discussed in section 4.3 corresponding to 0.01769 mol m^{-3}. Due to the uncertainty in the estimate of density change introduced by dissolved CH_4 we only discuss the results qualitatively. For CH_4 the density is lowered by a small fraction whereas for CO_2 the density is slightly increased. These opposite effects means that CO_2 will create stable density stratification when dissolved in seawaters. This will have a damping effect on vertical turbulence and thus also on vertical eddy diffusivity and viscosity. CH_4 on the other hand will have, if any, the opposite effect.

4.2.4 Dissolution rate

Mori and Mochizuki [1997] presented a general formula for dissolution of guest species to water. This is formulated as

$$J = \frac{1}{1-\tilde{C}_s}\left(K_w \frac{\rho_{w(g)}}{M_{w(g)}}(\tilde{C}_s - C_{amb}) - \frac{\tilde{C}_s}{1-\tilde{C}_s}J_w\right) \tag{2}$$

J is the flux given as mol m^{-2} s^{-1}. $K_w = u_* 0.1 Sc^{-0.67}$ is the mass transfer coefficient where u_* is the friction velocity and Sc is the Schmidt number ($Sc = \nu\alpha^{-1}$ where ν is

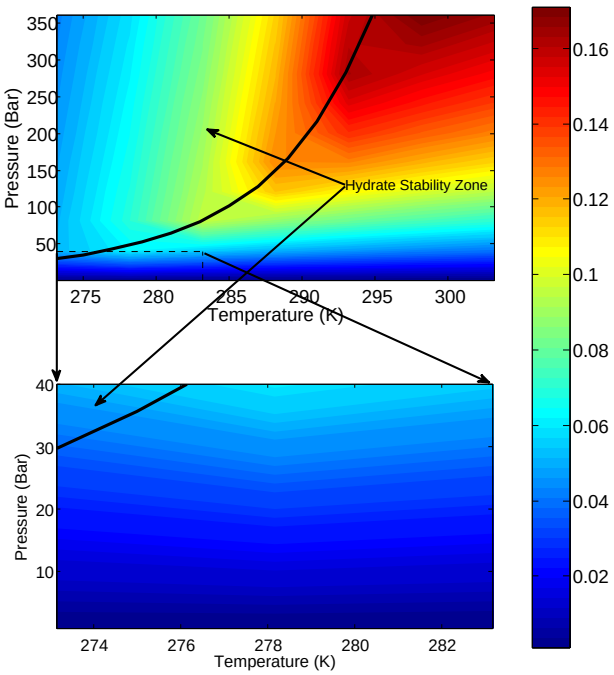

Figure 3: Solubility [molkg^{-1}] of CH_4 as a function of pressure and temperature with a zooming from 1 - 40 bar and 273.15 to 283.15 K.

viscosity and α is the mass diffusivity). $\rho_{w(g)}$ and $M_{w(g)}$ is the effective density and molar mass of water saturated with the dissolving substance. $\tilde{C}_s$ is the solubility and C_{amb} is the ambient concentration of the guest species. C_{amb} is usually much lower than $\tilde{C}_s$ so it can be neglected in the following. The effect of the last term is to account for the damping of the flux in presence of a hydrate layer where J_w is given as

$$J_w = \frac{r_c p}{\tau^2} \frac{\gamma cos(\phi)}{4\delta M_{w(g)} \nu_{w(g)}} (1 - \tilde{C}_s). \tag{3}$$

r_c is the capillary radius, p is the porosity, τ is the tortuosity, γ the interfacial tension, ϕ is the contact angle, $\nu_{w(g)}$ the viscosity and δ the thickness of the hydrate layer. This formula, builds on the micro perforated plate model shortly described in section (4.1.2).

We first look at equation (2), and ignore the extra term accounting for the hydrate effects. In this equation $M_{w(g)} = M_w(1 - \tilde{C}_s) + M_g \tilde{C}_s$. Keeping in mind that $\tilde{C}_s$ is a small number for the two gases in question $M_{w(g)}$ and $\rho_{m(g)}$ will only be slightly different from the values of pure water. E.g. $M_{w(g)}$ will only be 2.4 per mil higher for CO_2 and $\rho_{w(g)}$ 0.07 per mil ($P = 100\mathrm{bar}, \mathrm{T} = 4.2^{\mathrm{o}}\mathrm{C}$).

Assuming that the Sc numbers is approximately the same for CO_2 and CH_4 we are left with one determining factor for the dissolution rate. This is the solubility of CO_2 and CH_4. From this reasoning the ratio in the dissolution rate without a hydrate layer will follow the same line as given in Figure (4). Interestingly this is also the conclusion of Rehder et al. [2004]. They investigated the difference in dissolution rate from hydrate coated CO_2 and CH_4 bubbles from an in situ experiment.

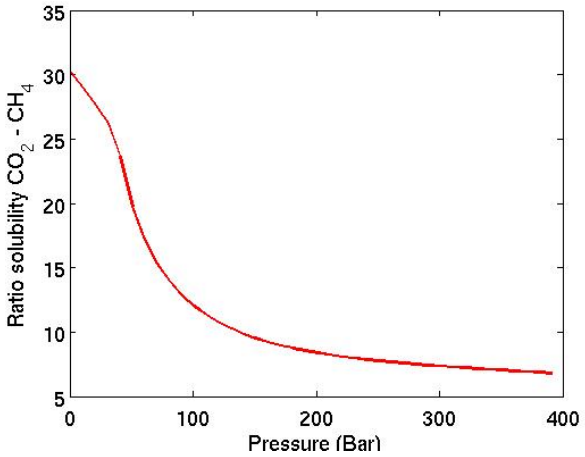

Figure 4: The ratio of the solubility of CO_2 and CH_4 at 277.35 K from 1 - 400 bar.

4.2.5 Hydrate Stability Zone

At low temperatures and high pressures water and gases is known to form hydrate (clathrate) consisting of water molecules cages with a guest molecule inside. The guest molecules could both be CO_2 or CH_4. Figure (5) displays the Hydrate Stability Zone (HSZ) for CO_2 and CH_4 in a temperature - pressure diagram. When computing HSZ the seawater is assumed to be saturated with CO_2 or CH_4. In the vicinity of gas bubbles or droplets the concentration of dissolved gas will be high compared to solubility, and the bubbles/droplets is reported to be coated with a hydrate layer up till the HSZ (Rehder et al. [2002]). In the computation a salinity of 35 psu is assumed. The lines are calculated based on Duan and Sun [2006].

For low temperatures CO_2 hydrate is stable for lower pressure than CH_4. At the point where the HSZ profile crosses the point where CO_2 becomes liquid, the HSZ curve of CO_2 changes drastically its profile. This leads to a much less temperature dependence of hydrate stability of CO_2 beyond this point. Thus at high temperatures CH_4 hydrate is more stable than CO_2 hydrate. For the temperature range at large depths in the ocean, however, both hydrate types are stable. At the temperature of 4 ^{o}C CO_2 hydrate will form at 23.018 bar whereas CH_4 hydrate will form at 43.976 bar.

4.2.6 Diffusivity and viscosity

Figure 6 shows the ratio between the molecular diffusivity in water and viscosity. The diffusivity is calculated based on "Jahne et al. [1987] and the viscosity on Trengove and Wakeham [1987]. The ratio close to one for the diffusivity should mean that the molecular diffusion should be the same. In the turbulent layer near the bottom the eddy diffusivity would typically be order of magnitudes larger than the molecular diffusivity. The viscosity is interesting to know in regard to subsurface flow and modelling in the porous media.

4.2.7 Bacteria oxidation of CH_4

In addition to the chemical differences there is an additional factor affecting the concentration of CH_4. In oxic conditions bacterias will oxidize methane via the reaction

$$CH_4 + 2O_2 \rightarrow CO_2 + H_2O$$

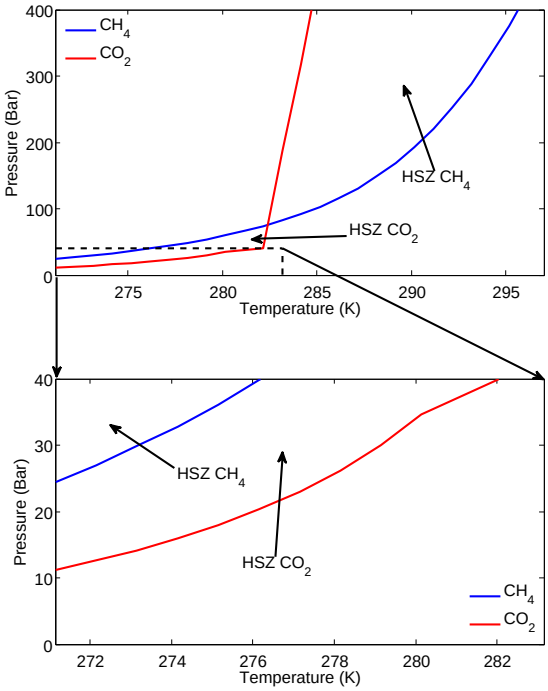

Figure 5: The hydrate stability zone in seawater as a function of temperature and pressure.

This introduces a sink term in the concentration of methane which might not be easy to account for. Some references report on how large this sink term is overall. Hovland et al. [1995] measured the methane concentration above a pockmark field east of Bear Island in the Barents sea. They find that the methane concentration is reduced by 98 percent within the water column from 300 meters depth to the sea surface by the biota. Cowen et al. [2002] looked at the methane originating from the Endeavour Segment at the Juan de Fuca Ridge, and found that there were extensive microbial methane oxidation. Less than 5 % of original hydrothermal methane remains in the plume at the station placed 15 km off-axis. Sauter et al. [2006] on the other hand report on low bacterial impact on the methane concentration. This might be due for that in the area of the deep-sea mud volcano Håkon Mosby, which they are looking at, the methane droplets are coated with hydrate and hence less accessible to bacterias. Scranton and McShane [1991] performed a study of the methane-rich area near the mouths of the rivers Rhine and Scheldt. They conclude that for the North Sea the sink of methane due to bacterial oxidation is relatively small compared to the gas loss to the atmosphere.

4.3 Observations of Methane plumes

Here we mention some of the reports on spreading of CH_4 above gas seepages. One very relevant article by Leifer and Judd [2002] investigate concentrations above a seepage field in the North Sea. Their hypothesis was that gas bubbles rising is creating a buoyant plume. When the gas bubbles are dissolved the buoyant force disappears, and this may lead to creation of a layer enriched in CH_4. The authors call this process bubble deposition. They

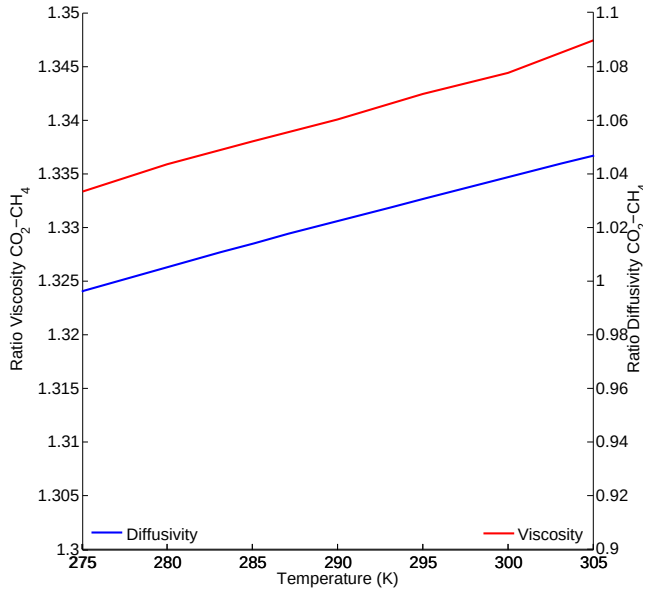

Figure 6: Ratio of viscosity [μ Pa s] and diffusivity [$m^2\ s^{-1}$] for CO_2 and CH_4.

measured CH_4 concentrations above a pockmark at a water depth of 175 m. The results show two distinct peaks in concentrations, one at 150 - 160 m depth and another at 100 - 125 m depth (See Figure 8). The lowest peak is explained by the authors as a result of sediment disturbance during water bottle casts. The other peak at 110 m depth is taken to account for the theory of bubble deposition. From the shallowest peak the concentration is gradually decreasing toward the surface. This peak seems to be around > 250 nl l^{-1} inside the plume.

Suess et al. [1999] made measurements at the Cascadia convergent margin. In this area hydrates is present in a convergent margin. These hydrates are destabilised at depth and free gas drives fluid upwards. Figure 7 shows the methane concentrations measured by the authors. The plume is reported to be hundreds of meters high and several kilometres wide. The concentration of methane was measured up till 74 000 nl l^{-1} which can be compared to the background levels of < 20 nl l^{-1} in the deep ocean and equilibrium value with respect to current atmospheric content of 57 nl l^{-1}. The authors found that the methane plume was restricted to depths below 400 m, which gives an impression that the process of bubble deposition also is present here.

4.3.1 Methane and Carbon Dioxide bubbles

Measurements of rising and dissolving CO_2 and CH_4 bubbles/droplets has been studied by in situ observations. Rehder et al. [2002] investigated rising CH_4 bubbles from the depth of 440 m to 830 m. This is both above and below the HSZ. They measured the shrinking rate of the bubbles and compared with the same rate for Argon bubbles. They found that the shrinking rate was consistent at all depths (mean 12.8 μm s^{-1} but below the HSZ the

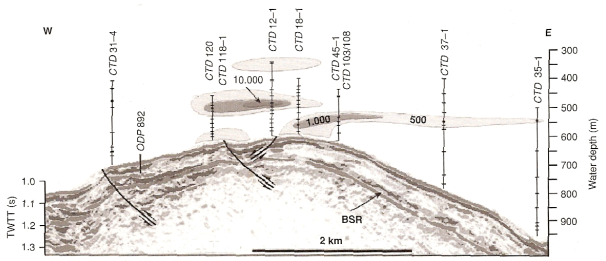

Figure 7: Methane plumes rising from the seabed at the Cascadia convergent margin Suess et al. [1999].

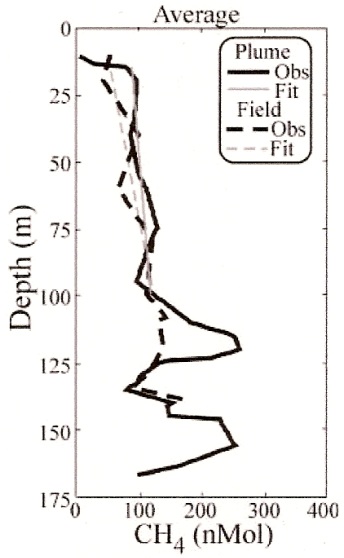

Figure 8: Averaged CH_4 concentrations above and distant from pockmarks fields in the North Sea Leifer and Judd [2002].

shrinking rate of CH_4 was significantly decreased (mean 3.0 μm s^{-1}). The rising rate of the CH_4 bubbles was found to be 29.2 $\pm$ 1.8 cm s^{-1}.

Brewer et al. [2002] performed similar experiments for CO_2 released from 800 m depth. They were able to follow the droplets for 400 m. This whole range should be below the HSZ for CO_2. The authors found that 90% of the mass loss occured during the ascent over the first 200 m. The rising rate was estimated to 10 cm s^{-1}. Also one of the results was that the dissolution rate was persistent 3.0 μmol cm^{-2} s^{-1}. A correlation for the mass transfer was obtained to be

$$\frac{dm}{dt} = -4\pi r_e^2 \rho_{CO_2} V_m \Gamma \tag{4}$$

where Γ is the dissolution rate, V_m the molar volume of CO_2, m is the mass, ρ_{CO_2} the density and r_e the equivalent radius. Later Gangstø et al. [2005] have compared Brewer et al. [2002] findings with theoretical results with fairly good agreement. One of the theoretical conclusions is that smaller droplets size will give larger CO_2 concentrations near the release depth.

An important question in the regard of gas leakage at the seabottom is how large fraction of the leaked gas will reach the seasurface and leak to the atmosphere. This is studied by McGinnis et al. [2006] by means of observations in the Black Sea and a bubble model. Echograms from the Black sea shows tall "flares" of rising CH_4 bubbles ($>$ 1300 m) from the seabottom. The bubble model take into account both the outflux of CH_4 and influx of e.g. O_2 during ascent of the bubble. They conclude that "significant methane transfer to the atmosphere is only possible from very shallow water depths, i.e., less than 100 m". They also state that that only catastrophic releases can give significantly outgassing to the atmosphere from deeper leakages ($>$ 100 m). Such a catastrophic release is shortly described in section 3.5.

4.4 Droplet modelling

To see the difference between CO_2 and CH_4 more quantitatively than what is shown in the previous sections we have employed a single droplet model previously used by Gangstø et al. [2005]. The rise and dissolution of the droplets are computed using the equations for terminal rise velocity and mass transfer. In this model the effect of hydrate layers is not accounted for. The equation for the drop terminal rise velocity is given as

$$U_T = \left(\frac{8gr_e(\rho - \rho_*)}{3C_d\rho} \right)^{0.5}, \tag{5}$$

where g is the gravitational acceleration, r_e is the equivalent radius, ρ is the seawater density, ρ_* is the density of the compound and C_d is the drag coefficient. Subscript * denotes the compound. The equation for mass transfer is

$$\frac{dm}{dt} = -Sh\pi d_e D_v M_*(C_s - C). \tag{6}$$

Sh is the Sherwood number, d_e [m] is the equivalent diameter, D_v [m^2/s] is the molecular diffusion coefficient, M_* [kg/mol] is the molecular mass of the gas species and C_s is set equal the solubility. The ambient gas concentration C is usually much lower than the solubility and can be neglected.

Figure 9 shows how the radius changes with depth for a drop/bubble released at 800 meters depth. The initial radius is varied between 4, 6, 8 and 10 mm. As is seen from the figure CO_2 is dissolved at a higher rate as suggested in the above discussion. For the 6 mm drop the CO_2 droplet rises from 800 meters depth to 726 meters depth whereas the CH_4 bubble rises to 432 meters. For methane bubbles with an initial radius of 10 mm the models gives the results that the bubbles will reach the surface.

In Figure 10 the terminal rise velocity is shown as a function of depth. Due to the larger density of CO_2 droplets the CH_4 bubbles are rising faster than the CO_2 droplets by a factor from 1.42 to 2.23 for 4 mm and 10 mm respectively in the initial phase..

4.5 Summary and preliminary conclusions

The observations and theoretical results presented is to sparse to conclude on the faith of a CO_2 leakage at the seabottom, but some indications may be found. Firstly the dissolution rate differences found in section 2 and hence the mass transfer (Equation 4) means that at the same side of the HSZ for both CH_4 and CO_2 a CO_2 bubble/droplet should be much faster dissolved. Data from a single drop model support this conclusion. At the same time dissolved CO_2 induces higher density whereas CH_4 has little or opposite effect. Based on the observations by Suess et al. [1999] and Leifer and Judd [2002] it should be possible to state that a similar leakage of CO_2 a major part of the gas should spread horizontally at lower depths. Also following the bubble deposition theory and considering the results for terminal rise velocity from the single drop model this also indicate that CO_2 will spread

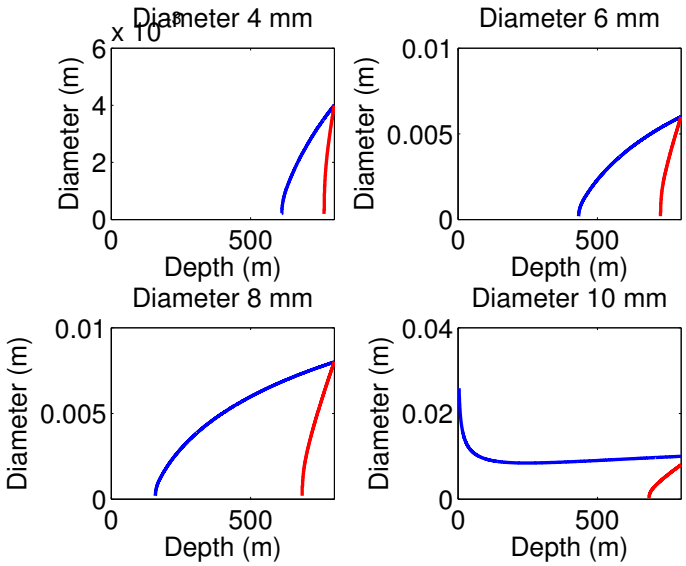

Figure 9: The development of the droplet radius as a function of depth for different initial radixes.

horizontally at lower depths than CH_4. In addition the increase in density introduced by dissolved CO_2 should enhance this effect. Stable density stratification will damp vertical turbulence and hence the vertical spreading. In the region where CO_2 forms hydrate and CH_4 does not (440 - 230 m) the mass transfer should be more similar. The maximum concentration found by Suess et al. [1999] was 74 000 nl l^{-1}. A similar concentration of CO_2 would give a pH reduction of 0.5. In view of the chemical features of CH_4 together with the fact that CH_4 is consumed by bacterias in oxic conditions this may be regarded as a lower bound of pH reduction for a similar CO_2 leakage. The results presented in section 4.3.1 indicates that the leakage has to be shallow if CO_2 should be transported by bubbles to the atmosphere. However this subject is more complicated because the upper winter mixed layer is ventilated on relatively short time scale.

4.6 Advantages and disadvantages

When choosing which system to look at in this project there are several arguments to consider. Some of the advantages of choosing CO_2 leakage near hydrothermal vents is that we are then studying the behaviour of CO_2 in seawater, and we will be able to model the pH reduction and the unique properties of CO_2. Since the difference in the features of CO_2 and CH_4 is so significant in seawater as documented in the previous section, it could be difficult to draw any further conclusions by studying CH_4 to the CO_2 case. Also since the CO_2 seems to accumulate in lakes beneath the seafloor a model could be relevant for other storage techniques such as ocean storage. Some of the disadvantages is that their locations at volcanic areas introduce the extra effect of large temperature gradients which would not be present at a geological storage site. It would probably also be a rather difficult task to give a realistic model of the hydrate layer on top of the CO_2 lake and the bubbling of CO_2 through this.

By modelling gas stream from pockmarks on the other hand it would most likely be more easy to make the reservoir model since this flow would be more similar to other reservoir models. Also there could be a possibility to make in situ measurement as needed as the location of pockmarks is national and collaborators are studying pockmarks in situ.

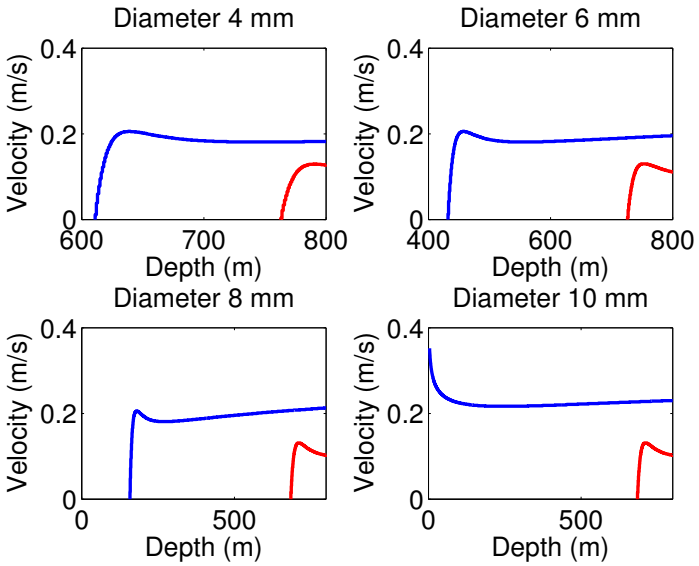

Figure 10: The development of the terminal rise velocity as a function of depth.

There is also the possibility that there could be a part of CO_2 in the gases leaked from the pockmarks since this has not been measured so far. This could open the possibility to include other collaborators from the university into the investigation. A simulation tool could also be a good starting point to model pockmarks as a seabed phenomenon. On the contrary as already mentioned, the analog of CH_4 and CO_2 in seawater is rather poor. Also the oxidation of CH_4 by bacterias introduces an added difficulty and effect compared to simulation of CO_2 leakage. It is unknown whether CO_2 is present in the seepage from pockmarks and if it is, we would have to also take into account the other gases when studying the dissolution and transport in seawater. A study of pockmarks would probably put the focus from what is happening above the seafloor to what is happening below the seafloor.

Acknowledgment
This work has been supported by Norwegian Academy of Science and Letters and Statoil through VISTA (6152).

References

P. G. Brewer, E. T. Peltzer, G. Friederich, and G. Rehder. Experimental determination of the fate of rising CO_2 droplets in seawater. *Environ. Sci. Technol.*, 36:5441–5446, 2002. 4.3.1, 4.3.1

J. F. Clark, L. Washburn, J. S. Harnafius, and B. P. Luyendyk. Dissolved hydrocarbon flux from natural marine seeps to the southern California Bight. *J. Geophys. Res.*, 105(C5): 11509–11522, 2000. 3.2

J. P. Cowen, X. Wen, and B. N. Popp. Methane in aging hydrothermal plumes. *Geochimica et Cosmochimica Acta*, 66(20):3563–3571, 2002. 4.2.7

P. R. Dando, J. A. Hughes, and Y. *et al.* Leahy. Gas venting from submarine hydrothermal areas around the island of Milos, Helelnic Volcanic Arc. *Cont. Shelf Res.*, 15:913–929, 1995. 2.5

A. Demurov, R. Radhakrishnan, and B. L. Trout. Computations of diffusivities in ice and CO_2 clathrate hydrates via molecular dynamics and Monte Carlo simulations. *J. Chem. Phys.*, 116(2):702–710, 2002. 4.1.3

ZH. Duan and S. Mao. A thermodynamic model for calculating methane solubility, density and gas phase composition of methane-bearing aqueous fluids from 273 to 523 K and from 1 to 2000 bar. *Geochimica et Cosmochimica Acta*, 70:3369–3386, 2006a. 4.2.2, 4.2.3

ZH. Duan and S. Mao. An improved model for the calculation of CO_2 solubility in aqueous solutions containing Na^+, K^+, Ca^+, Mg^{2+}, Cl^-, and ${SO_4}^{2-}$. *Marine Chem.*, 98:131–139, 2006b. 4.2.2

ZH. Duan and R. Sun. A model to predict phase equilibrium of CH_4 and CO_2 clathrate hydrate in aqueous electrolyte solutions. *Amer. Mineral.*, 91(8-9):1346–1354, 2006. 4.2.5

R. Gangstø, P. M. Haugan, and G. Alendal. Parameterization of drag and dissolution of rising CO_2 drops in seawater. *Geophys. Res. Letters*, 32:L10612, 2005. 4.3.1, 4.4

M. Hovland. On the self-sealing nature of marine seeps. *Cont. Shelf Res.*, 22:2387–2394, 2002. 3.4

M. Hovland and A. G. Judd. *Seabed Pockmarks and Seepages*. Graham & Trotman, 1988. 3, 3.4

M. Hovland, A. G. Judd, and Jr. R. A. Burke. The global flux of methane from shallow submarine sediments. *Chemosphere*, 26:559–578, 1993. 3.2

M. Hovland, E. Suess, and M. Hovland. A large methane plume east of Bear Island (Barents Sea): implications for the marine methane cycle. *Geol. Rundsch.*, 84:59–66, 1995. 4.2.7

F. Inagaki, M. M. M. Kuypers, U. Tsunogai, Ishibashi J., K. Nakamura, T. Treude, S. Ohkubo, M. Nakaseama, K. Gena, H. Chiba, H. Hirayama, T. Nunoura, K. Takai, B. B. Jœrgensen, K. Horikoshi, and A. Boetius. Micobial community in a sediment-hosted CO_2 lake of the southern Okinawa Trough hydrothermal system. *Proceedings of the National Academy of Science of the United States of America*, 103: 14164–14169, 2006. 2.3, 4.1.4

M. Ivanov, G. K. Westbrook, V. Blinova, E. Kozlova, A. Mazzini, H. Nouze, and Minshull T. A. First sampling of gas hydrate from the Vøring plateau. *EOS*, 88(19): 209–216, 2007. 3.3

B. "Jahne, G. Heinz, and W." Dietrich. Measurement of the diffusion coefficients of sparingly soluble gases in water. *J. Geophys. Res.*, 92(C10):10767–10776, 1987. 4.2.6

A. G. Judd and M. Hovland. *Seabed Fluid Flow*. Cambridge, 2007. 2, 2.6, 2.7

D. M. Karl, A. McMurtry, A. Malahoff, and M. O. Garcia. Loihi Seamount Hawaii: A mid-plate volcano with a distinctive hydrothermal system. *Nature*, 335:532–535, 1988. 2.4

L. H. King and B. MacLean. Pockmarks on the Scontian Shelf. *Geol. Soc. Am. Bull.*, 81: 3141–3148, 1970. 3.1

U. Konno, U. Tsunogai, F. Nakagawa, M. Nakeasema, J. Ishibashi, T. Nunoura, and K. Nakamura. Liquid CO_2 venting on the seafloor: Yonaguni Knoll IV hydrothermal system, Okinawa Through. *Geophys. Res. Letters*, 33, 2006. 2.3

K. A. Kvenvolden, C. H. Nelson, and D. R. et al. Thor. Biogenic and thermogenic gas in gas-charged sediments of Norton Sound, Alaska. In *Proceeding of the Offshore Technology Conference*, page 3412. OTC paper, 1979. 2.7

I. Leifer, J. Boles, and B. Luyendyk. Measurments of Oil and Gas emissions from a marine seep. *EDT-009*, 2007. 3.2

I. Leifer and A. G. Judd. Oceanic methane layers: the hydrocarbon seep bubble deposition hypothesis. *Terra Nova*, 2002. 4.3, 8, 4.5

J. Lupton, D. Butterfield, M. Lilley, Evans L., K. Nakamura, W. Jr. Chadwick, J. Resing, R. Embley, E. Olson, G. Proskurowski, E. Baker, C. de Ronde, K. Roe, R. Greene, G. Lebon, and C. Young. Venting of carbon dioxide-rich fluid and hydrate formation in Mid-Okinawa Through Backarc Basin. *Science*, 248(4959):1093–1096, 2006. 2.2

D. F. McGinnis, J. Greinert, Y. Artemov, S. E. Beaubien, and A. W $u$est. Fate of rising methane bubbles in stratified waters: How much methane reaches the atmosphere? *J. Geophys. Res.*, 111:C09007, 2006. 4.3.1

Y. H. Mori and T. Mochizuki. Mass transport across clathrate hydrate films - a caplillary permeation model. *Chem. Eng. Sci.*, 52:3613–3616, 1997. 4.1.2, 4.2.4

C. H. Nelson, D. R. Thor, and M. W. Sanstrom. Modern biogenic gas-generated craters (sea floor 'pockmarks') on the Bering Shelf, Alaska. *Geological Society of America (Bulletin)*, 90:1144–1152, 1979. 2.7

R. Radhakrishnan, A. Demurov, H. Herzog, and B. L. Trout. A consistent and verifiable macroscopic model for the dissolution of liquid CO_2 in water under hydrate forming conditions. *Energy Conversion and Management*, 44:771–780, 2003. 4.1.3

G. Rehder, P. W. Brewer, E. T. Peltzer, and G. Friederich. Enhanced lifetime of methane bubble streams within the deep ocean. *Geophys. Res. Letters*, 29(15), 2002. 4.2.5, 4.3.1

G. Rehder, R. S. Keir, E. Suess, and T. Pohlmann. The multiple sources and patterns of methane in North Sean waters . *Aqua. Geochem.*, 4:403–427, 1998. 3.5

G. Rehder, S. H. Kirby, W. B. Durham, L. A. Stern, E. T. Peltzer, J. Pinkston, and P. G. Brewer. Dissolution rates of pure methane hydrate and carbon-dioxide hydrate in undersaturated seawater at 1000-m depth. *Geochimica et Cosmochimica Acta*, 68(2): 285–292, 2004. 4.2.4

P. Rensbergen, A Rabaute, A. Colpaert, M. Ghislain, T. St. Mathijs, and A. Bruggeman. Fluid migration and fluid seepage in the Connemara Field, Porcupine Basin interpreted from industrial 3D seismic and well data combined with high-resolution site survey data. *Int. J. Earth Sci.*, 96:185–197, 2007. 3.3

H. Sakai, T. Gamo, E-S Kim, Tsutsumi M., T. Tanaka, J. Ishibashi, H. Wakita, M. Yamano, and T. Oomori. Submarine venting of liquid carbon dioxide on a Mariana Arc volcano. *Geochem. Geophys. Geosys.*, 7(8):1525–2027, 1990. 2.1

E. J. Sauter, S. I. Muyakshin, J-L. Charlou, M. Schluter, A. Boetius, K. Jerosch, E. Damm, J-P. Foucher, and Klages M. Methane discharge from a deep-sea submarine mud volcano into the upper water column by gas hydrate-coated methane bubbles. *Earth and Planetary Science Letters*, 243:354–365, 2006. 4.2.7

M. I. Scranton and K. McShane. Methane fluxes in the southern North Sea: the role of European rivers. *Cont. Shelf. Res.*, 11:37–52, 1991. 4.2.7

P. N. Sedwick, G. M. McMurty, and J. D. MacDougall. Chemistry of hydrothermal solutions from Pele's Vents, Loihi Seamount, Hawaii. *Geochim. Cosmochim. Acta*, 56: 3643 – 3667, 1992. 2.4

Y. Shindo, P. C. Lund, Y. Fujioka, and H. Komiyama. Kinetics and mechanism of the formation of CO_2 hydrate. *Int. J. Chem. Kinet.*, 25(9):777–782, 1993. 4.1.1

E. Suess, M. E. Torres, G. Bohrmann, R. W. Collier, J. Greinert, P. Linke, G. Rehder, A. Trehu, K. Wallman, G. Winckler, and E. Zuleger. Gas hydrate destabilization: enhanced dewatering, benthic material turnover and large methane plumes at the Cascadia convergent margin. *Earth and Planetary Science Letters*, 170:1–15, 1999. 4.2.3, 4.3, 7, 4.5

R. D. Trengove and W. A. Wakeham. The viscosity of carbon dioxide, methane, and sulfur hexafluorid in the limit of zero density. *Chem. Ref. Data*, 16:175–187, 1987. 4.2.6

E. W. Vetter and C. R. Smith. Insight into the ecological effects of deep ocean CO_2 enrichment: The impacts of natural CO_2 venting at Loihi seamount on deep sea scavengers. *J. Geophys. Res.*, 110:C09S13, 2005. 2.4

L. Zuhlsdorff and V. Spiess. Three-dimensional seismic characterization of a venting site reveals compelling indications of natural hydraulic fracturing. *Geology*, 32(2):101–104, 2004. 3.4